

BUILDING COMPONENT DEFORMATION TRACKING USING STRUCTURED LIGHT TECHNIQUE

Shuang Zhao¹, Chun Liu^{1,2}*, Jing Zhang²

¹ College of Surveying and Geo-informatics, Tongji University, Shanghai 200092, China- (liuchun, zhaoshuang)@tongji.edu.cn

² Urban Mobility Institute, Tongji University, Shanghai 200092, China- jingzh@tongji.edu.cn

Commission II, WG II/8

KEY WORDS: Deformation Tracking, Structured Light Technique, 3D Full-field Optical Measurement, Non-contact, Building Component, Displacement Field.

ABSTRACT:

It is crucial to fully master the mechanical properties of building components for ensuring the safety of infrastructures during service. The laboratory deformation test is an important way to study the mechanical properties of building components. At present, there is still a lack of a combination of high-efficiency, high-accuracy, and low-cost measurement methods for laboratory deformation tests. To address the issue, a method is proposed to measure the deformation of building components by using the structured light technique in this paper. It is applied to the axial tensile test of the dog-bone specimen, and the 3D full-field displacement of the dog-bone specimen is obtained by calculating the established deformation tracking model. The experimental results demonstrate the deformation measurement accuracy is at the millimeter level and can meet the accuracy requirement in the laboratory. Furthermore, the results are consistent with the way of force and the deformation mechanism of the dog-bone specimen. This paper presents a novel method for the deformation measurement, which provides a reliable analysis basis for studying the mechanical properties of building components.

1. INTRODUCTION

In recent years, the development of infrastructure construction has risen rapidly, along with more and more safety incidents, such as bridge failures, building collapses, etc. These incidents may cause significant property losses and even casualties (Milillo et al., 2019). Therefore, we need to pay more attention to the safety issues of infrastructure. Fully mastering the mechanical properties of building components to select suitable design schemes is of great significance for ensuring the safety of infrastructures during service. It is an important way to study the mechanical properties of building components by the laboratory deformation test. The behavior and characteristics of building components under load can be mastered by observing the deformation under external forces such as tension, compression, shear, torsion, and bending (Hareendran et al., 2019).

In-plane and out-of-plane deformation is typically observed during tests (Han and Huang, 2009; Palieraki et al., 2018). The laboratory deformation measurement techniques can be divided into two classes: contact measurement and non-contact measurement, according to whether they contact the measured object or not. The traditional contact measurement techniques deploy extensometers or strain gauges, etc. on the surface of the measured object, which usually require multiple laying points (Motra et al., 2014). Nonetheless, full-field deformation cannot be obtained. In addition, equipment like strain gauges may fall off when the measured object deforms to crack. At present, the non-contact measurement technique widely uses the optical measurement techniques assisted by digital image correlation (DIC) (Peters and Ranson, 1982; Yamaguchi, 1981), which includes two-dimensional digital image correlation (2D-DIC) and three-dimensional digital image correlation (3D-DIC) (Pan, 2018). The 2D-DIC method using a single fixed camera is limited to in-plane deformation measurement of flat surface objects (Pan et al., 2009). Compared with the 2D-DIC method, the 3D-DIC method using two cameras can also measure the out-of-plane

deformation (Pan et al., 2018). However, if high dense matching is to be achieved, the computational cost of 3D reconstruction based on template matching will be very high. Furthermore, in order to achieve real-time monitoring, hardware with high performance is required, which increases the cost of the entire system. In summary, there is still a lack of a measurement method that combines high efficiency, high accuracy, and low cost for building components deformation tests.

In this paper, a novel method that uses the structured light technique is proposed to address the above issues. Specifically, a binocular structured light system (Fig. 1) is employed, which consists of a Digital Light Processing (DLP) projector and two cameras. It has the advantages of high feasibility and high reliability (Han and Huang, 2009).

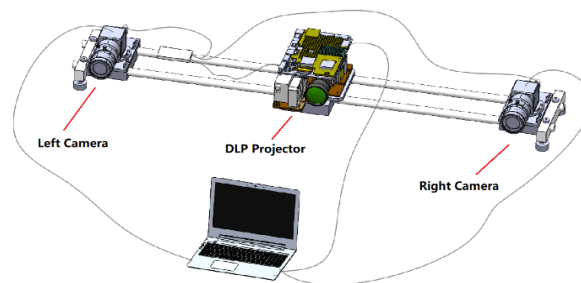


Figure 1. Binocular structured light system consisting of a DLP projector and two cameras.

The remainder of this paper is organized as follows. Section 2 introduces the framework of the proposed method, where we also describe the main principles involved. Section 3 presents the experimental settings and results. Finally, the conclusions are given in Section 4.

* Corresponding author

2. METHODOLOGY

2.1 Overview

As demonstrated in Figure 2, the general framework of the proposed method is mainly comprised of four parts: data collection, data pre-processing, deformation tracking, and visualization. The detailed description is as follows.

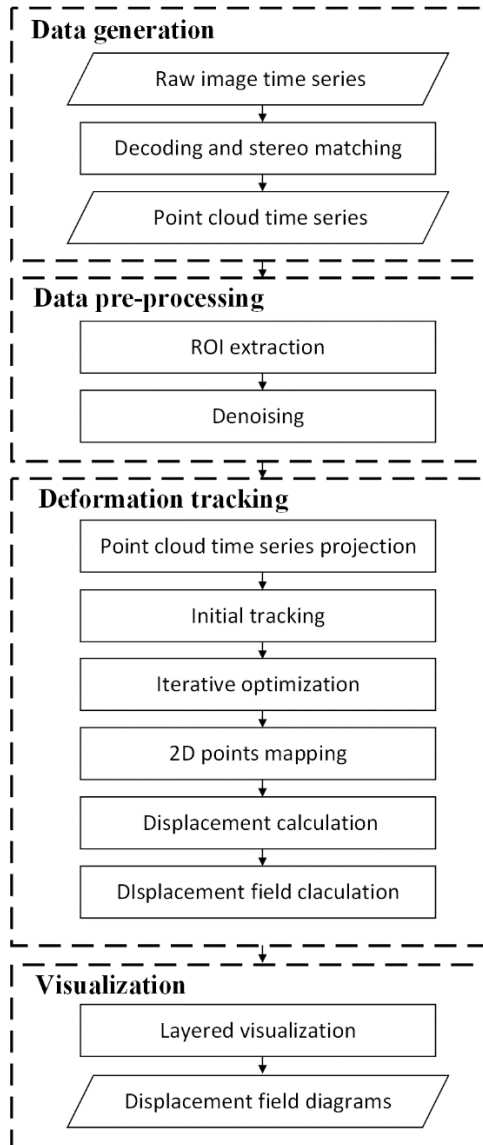


Figure 2. Flowchart of the proposed method.

1. Data collection: The binocular structured light system is applied to capture images to generate point cloud time series. The DLP projector actively projects a series of encoded patterns on the surface of building components sequentially. The geometry of the building components deforms the patterns, which are sequentially captured by left and right cameras from different viewpoints simultaneously. These images form the raw image time series according to the order of acquisition time. After decoding and stereo matching of image time series, the multi-frame point cloud with the 3D coordinates and grayscale are generated and form point cloud time series.

2. Data pre-processing: The raw point cloud contains background data and noise data, which needs pre-processing. The

background data does not belong to the region of interest (ROI) of the deformation tracking. The noise data interfere with deformation tracking and affect the accuracy of displacement calculation results. Therefore, filtering and cropping are used to remove the background data to extract the ROI region. To eliminate the noise data, the Random Sample Consensus (RANSAC) algorithm is employed.

3. Deformation tracking: The deformation tracking aims at calculating deformation by matching 3D deformation points. First of all, the point cloud time series is projected into image time series. The correlation function based on the grayscale is used to initially track points in the image time series. The initial tracking points are iteratively optimized to obtain more accurate 2D tracking points. Afterwards, they are respectively mapped to 3D points to calculate displacement. Finally, the displacement field is obtained by interpolating the calculated displacement.

4. Visualization: The displacement field visualization can directly display the deformation regularity of the measured object. The visualization diagrams are divided into two layers. The first visual layer uses the scalar field visualization method of color mapping to visualize the displacement values. The second visual layer uses the vector field visualization method to visualize the direction of displacement. Finally, the displacement field diagrams are generated by overlaying the two visual layers.

Furthermore, the main principles involved in the proposed framework are introduced in the following subsections.

2.2 Point Cloud Generation

Similar to traditional stereo vision, the binocular structured light system uses the corresponding image points (CIPs) in the left and right image pairs to generate point cloud based on the principle of triangulation. Assuming that the left camera coordinate system is the world coordinate system, the 3D coordinates of the points can be obtained by solving the following formulas using the least squares method.

$$Z_w \begin{bmatrix} u_l \\ v_l \end{bmatrix} = I_l \begin{bmatrix} X_w \\ Y_w \\ Z_w \end{bmatrix} \quad (1)$$

$$Z_w \begin{bmatrix} u_r \\ v_r \end{bmatrix} = I_r [R|T] \begin{bmatrix} X_w \\ Y_w \\ Z_w \end{bmatrix} \quad (2)$$

where u_l, v_l, u_r, v_r = pixel coordinates of the CIPs
 I_l, I_r = camera intrinsic matrix
 R, T = camera extrinsic matrix
 X_w, Y_w, Z_w = world coordinates of the points

It is expensive for the computational cost to solve the above formulas directly. As a result, stereo rectifying the left and right images is of great significance and greatly simplifies the calculation. The stereo rectification makes the actual binocular system close to the ideal binocular system. It means the CIPs only exist in aligned rows, resulting in the search space of CIPs being compressed from the whole image into a straight line.

Compared with traditional stereo vision, the binocular structured light system projects encoded patterns to add additional constraint information which assists with the search of CIPs (Fig. 3). Specifically, encoded patterns provide unique encoded value as a vertical constraint, which improves the efficiency of matching the CIPs.

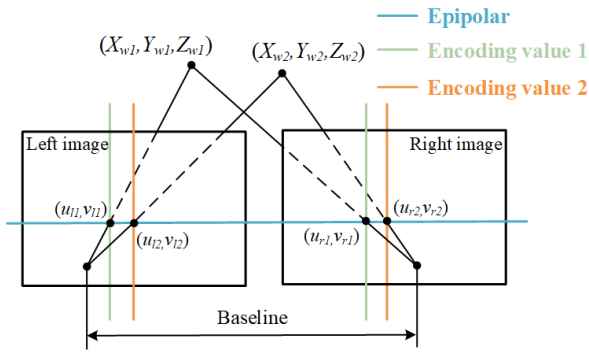


Figure 3. The bidirectional constraint.

Structured light patterns can be encoded in many ways. According to the encoding strategy, the patterns can be generally classified into multiple-shot and single-shot (Geng, 2011). One of the most widely used strategies is based on the multiple-shot strategy due to its advantages of high accuracy, strong robustness, and easy implementation (Chen et al., 2010). With the rapid development of high-speed projectors and cameras in recent years, the multiple-shot strategy is no longer limited to static scenes (Zhang, 2018).

The multiple-shot strategy can be further classified into four broad categories: Binary code, Gray code, phase shift, and hybrid method (Geng, 2011). Among them, the hybrid method combining Gray code and phase shift takes advantage of different methods to improve measurement accuracy and efficiency. In this method, the Gray Code is used to guide phase unwrapping, but sometimes the ambiguity at the junction of black and white may lead to failure. To solve the problem, the complementary Gray code method often replace the traditional Gray code in the hybrid method can ensure the reliability of phase unwrapping (Zhang et al., 2012).

The point cloud generated by the above principle only contains 3D coordinates information. The encoded patterns projected by the DLP projector overlay the surface texture of the building components, which is significant for subsequent 3D deformation point tracking in Section 2.3.2. So we need to use some grayscale restoration methods to generate point cloud with grayscale information, such as the modulation of captured phase-shifting fringe patterns (Wu et al., 2021).

2.3 Deformation Tracking

2.3.1 Point Cloud Projection

Along the line of sight of the left or right camera, the point cloud is projected to the imaging plane to reduce the dimension into an image. The transformation formula of point cloud projection can be expressed as follows:

$$\begin{bmatrix} x \\ y \\ 1 \end{bmatrix} = M \begin{bmatrix} R & T \\ 0 & 1 \end{bmatrix} \begin{bmatrix} X_w \\ Y_w \\ Z_w \\ 1 \end{bmatrix} \quad (3)$$

where x, y = image coordinates
 M = camera projection matrix
 R, T = camera extrinsic matrix.

The pre-processed point cloud time series is projected into the image time series and a mapping relationship between the 2D points and the 3D points is established at the same time. The formula can be expressed by the following formula:

$$\begin{cases} X_w = f_x(x, y) \\ Y_w = f_y(x, y) \\ Z_w = f_z(x, y) \end{cases} \quad (4)$$

where f_x, f_y, f_z = mapping functions between 2D points and 3D points in the X, Y - and Z -axis

2.3.2 3D Deformation Point Tracking

In the image time series, the first image is selected as the reference image, and subsequent images are treated as the deformed image. We select the starting point P_0 in the reference image and set the appropriate step size L to search the interest points. Furthermore, we take each interest point as the center to construct an area of a certain size as the reference subregions, and the coordinates of each point in the reference subregions also can be expressed as:

$$\begin{cases} x = x_0 + \Delta x \\ y = y_0 + \Delta y \end{cases} \quad (5)$$

where x_0, y_0 = image coordinates of the center points of the reference subregions
 $\Delta x, \Delta y$ = the increment of the points in the reference subregions relative to (x_0, y_0)

For each interest point in the reference image, we construct its corresponding candidate points in the deformed images, where the coordinates of each candidate point can be expressed as:

$$\begin{cases} x_0^* = x_0 + u \\ y_0^* = y_0 + v \end{cases} \quad (6)$$

where x_0^*, y_0^* = image coordinates of the candidate points
 u, v = the increment of the (x_0, y_0) relative to (x_0^*, y_0^*)

We also take each candidate point as the center and construct an area of a certain size as the deformed subregions, and each point in the deformed area can be expressed as:

$$\begin{cases} x^* = x_0 + u + u_x \Delta x + u_y \Delta y \\ y^* = y_0 + v + v_x \Delta x + v_y \Delta y \end{cases} \quad (7)$$

where x^*, y^* = image coordinates of the points in the reference subregions
 u_x, u_y, v_x, v_y = the gradient of u and v in the x and y directions

In order to calculate the correlation between the reference subregions and its corresponding deformed subregions, the deformation parameters \mathbf{p} and the correlation coefficient are used to construct the correlation function $C_{ZNSSD}(\mathbf{p})$. The Zero-normalized sum of squared differences (ZNSSD) correlation coefficient is robust, reliable and insensitive to the variation of intensity before and after deformation (Zhao et al., 2019), so it is highly recommended for practical use. The correlation function can be expressed as:

$$C_{ZNSSD}(\mathbf{p}) = \sum_{\Omega} \left[\frac{F(x, y) - \bar{F}}{\sqrt{\sum_{\Omega} (F(x, y) - \bar{F})^2}} - \frac{G(x^*, y^*) - \bar{G}}{\sqrt{\sum_{\Omega} (G(x^*, y^*) - \bar{G})^2}} \right]^2 \quad (8)$$

$$\mathbf{p} = [u \quad v \quad u_x \quad u_y \quad v_x \quad v_y] \quad (9)$$

where Ω = all the points in the reference subregions
 $F(x, y), G(x^*, y^*)$ = the grayscale of points in the reference and deformed subregions

\bar{F}, \bar{G} = the mean grayscale of the points in the reference and deformed subregions
 \mathbf{p} = deformation parameters which describes the shape change of the subregions

We set the threshold C_0 of the correlation index, when C_{ZNSSD} reaches the maximum value and is greater than the C_0 , the candidate point is regarded as the initial deformation tracking point of the interest point.

After obtaining the initial deformation tracking results, it is iteratively optimized by using the inverse-compositional Gauss-Newton (IC-GN) algorithm to achieve high-accuracy results. Then the final deformation tracking results are mapped to 3D points respectively according to Eq. (4) to establish the relationship of 3D deformation point tracking.

2.3.3 Deformation Calculation

We calculate the distance between a 3D point and its corresponding tracking point according to the established relationship of 3D deformation point tracking, which is regarded as the displacement values in the X -, Y - and Z -axis. The formula is shown in the following:

$$\begin{cases} U = f_x(x^*, y^*) - f_x(x, y) \\ V = f_y(x^*, y^*) - f_y(x, y) \\ W = f_z(x^*, y^*) - f_z(x, y) \end{cases} \quad (10)$$

where U, V, W = displacements of a 3D point in the X -, Y - and Z -axis

The displacement field is obtained by interpolating based on the displacement of 3D points, which describes the spatial distribution of the displacement on the surface of the building components and can characterize the deformation.

3. EXPERIMENT AND RESULTS

3.1 Experimental Setup

To demonstrate the applicability of the proposed method, we applied the binocular structured light system to the axial tensile test of the typical dog-bone specimen shown in Figure 4(a), which is used to simulate the deformation of building components in the laboratory. The test was carried out in a laboratory with uniform ambient light, as shown in Figure 4(b).

Before the test, speckles of uniform size and moderate density were prepared on the surface of the dog-bone specimen to enhance the texture for deformation tracking, and the two extensometers were installed on the left and right sides of the dog-bone specimen respectively, as shown in Figure 4(c). During the test, the lower part of the dog-bone specimen was fixed. The tensile force was applied on its upper part and its middle section would be elongated. The binocular structured light system continuously collected the left and right image pairs based on which we generated the point cloud time series with a time interval of 20s. The data of the two extensometers were also recorded at the same time. It is worth mentioning that the length of the measured area in the middle of the dog-bone specimen is 80 mm.

In the binocular structured light system, the DLP projector (DLP4710) has a resolution of 1920×1080 pixels and its frequency is 437Hz. The two cameras (MV-CA050-20UM) have a resolution of 1920×1080 pixels and their frequency is 70Hz.

All the camera intrinsic and extrinsic parameters were calibrated based on the Zhang's calibration method (Zhang, 1999). By the way, the dog-bone specimen was placed in an overlapping area of the field of view of the three sensors. In this case, we used the encoding strategy based on hybrid method. The DLP projector projected the 7-bit gray-code patterns, the complementary gray-code pattern and the 3-step phase-shift patterns with 128 phase fringes onto the dog-bone specimen in turn.

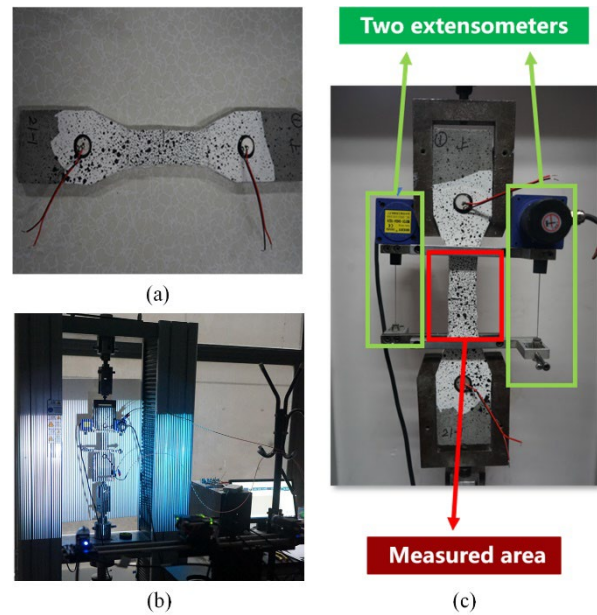


Figure 4. Deformation test component and scene. (a) Dog-bone specimen. (b) Axial tensile test environment. (c) Two installed extensometers.

3.2 Experimental Results

We estimated the accuracy of the proposed method by difference comparison with the measured true value of the deformation of the dog-bone specimen. Considering the possible errors of the extensometer, the mean value of the data measured by two extensometers was selected as the measured true value.

The absolute values of the specific displacement deviation during the test are listed in Table 1. The average displacement deviation is 0.6121mm. The deformation measurement accuracy is at the millimeter level and can meet the accuracy requirement in the laboratory.

Measurement time (s)	Displacement deviation (mm)
20	0.9649
40	0.7960
60	1.0520
80	0.6867
100	0.8257
120	0.5951
140	0.5141
160	0.4459
180	0.4290
200	0.6427
220	0.3020
240	0.1106
260	0.5921

Table 1. Difference comparison of deformation measured by the binocular structured light system and two extensometers.

We calculated and visualized the 3D full-field displacement of the dog-bone specimen, as shown in Figure 5. Figure 5(a) is the in-plane displacement vector fields, and Figure 5(b) is the out-of-plane displacement fields.

The displacement field visualization results demonstrate certain deformation regularity. As shown in Figure 5(a), the in-plane displacement of the measured area is relatively small in the early stage. As time goes by, the deformation continues and the in-plane displacement becomes larger and larger. In addition, affected by the way of force, the in-plane displacement becomes

increasingly larger from bottom to top, and the directions of in-plane displacement in the three stages are generally consistent with the direction of the tensile force. Since the force on the dog-bone specimen was almost vertically upward along the surface of it, the out-of-plane displacement in the three stages is relatively small and it also changes very little, as shown in Figure 5(b).

Therefore, the results are consistent with the way of force and the deformation mechanism of the dog-bone specimen, further demonstrating the effectiveness of the proposed method.

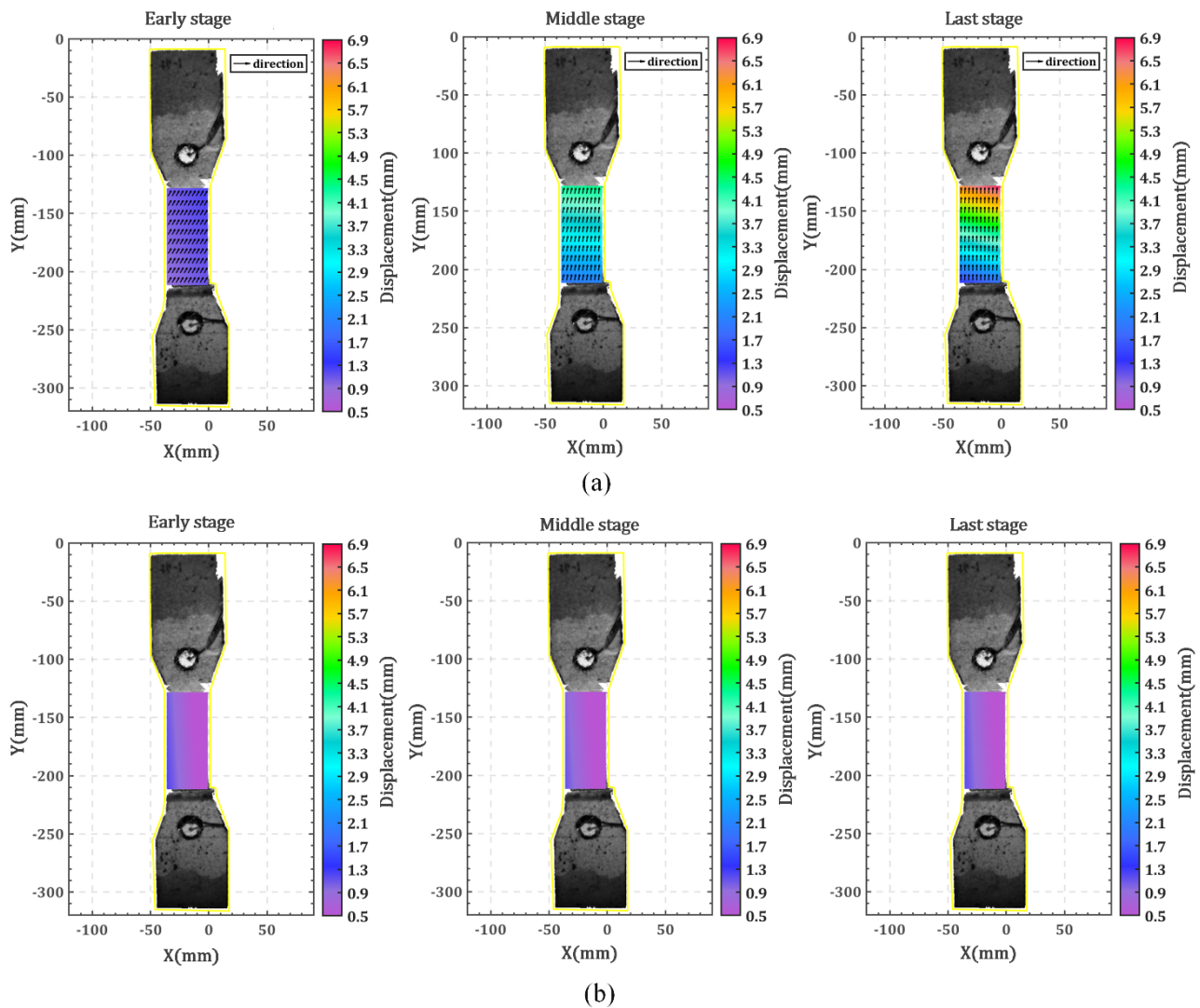


Figure 5. The displacement field of dog-bone specimen in two directions in the early, middle and last stage of deformation. (a) In-plane displacement vector fields. (b) Out-of-plane displacement fields.

4. CONCLUSION

Fully mastering the mechanical properties of building components is critical to ensure the safety of infrastructure during service. The binocular structured light system is applied to the axial tensile test of the dog-bone specimen in this paper. It solves the issue that the current deformation measurement techniques in the laboratory lack a combination of high-efficiency, high-accuracy, and low-cost methods. In addition, the deformation tracking model is established by using the correlation function and the iterative optimization method to calculate deformation accurately. The experimental results show that the deformation

measurement accuracy of our method is at the millimeter level, which can provide a reliable analysis basis for studying the mechanical properties of building components.

However, there are still several issues that need to be further studied. The deformation measurement accuracy is not only related to the deformation tracking algorithm but also related to the quality of the point cloud generated from the images collected by the binocular structured light system. Therefore, the optimization of the deformation tracking algorithm and the measurement error analysis of binocular structured light system will be our future research content. Furthermore, we will also

consider applying it to measure the deformation of reinforced concrete structural elements in the future.

ACKNOWLEDGEMENTS

This work was supported by the Major Program of the National Natural Science Foundation of China (Grant No. 42130106) and the "Science and Technology Innovation Action Plan" project of the Science and Technology Commission of Shanghai Municipality (20XD1403800).

REFERENCES

Chen, Y., Zuo, W., Wang, K., Wu, Q., 2010. Survey on Structured Light Pattern Codification Methods. *Mini Micro Systems*, 31(9), 1856-1863.

Geng, J., 2011. Structured-Light 3d Surface Imaging: A Tutorial. *Advances in Optics and Photonics*, 3, 128-160.

Han, X., Huang, P., 2009. Combined Stereovision and Phase Shifting Method: A New Approach for 3-D Shape Measurement. *Proceedings of SPIE - The International Society for Optical Engineering*, 7389, 1038-1045.

Hareendran, S.P., Reddy Kothamuthyala, S., Thammishetti, N., Suriya Prakash, S., 2019. Improved Softened Truss Model for Reinforced Concrete Members under Combined Loading Including Torsion. *Mechanics of Advanced Materials and Structures*, 26(1), 71-80.

Milillo, P., Giardina, G., Perissin, D., Milillo, G., Coletta, A., Terranova, C., 2019. Pre-Collapse Space Geodetic Observations of Critical Infrastructure: The Morandi Bridge, Genoa, Italy. *Remote Sensing*, 11(12), 1403-1416.

Motra, H.B., Hildebrand, J., Dimmig-Osburg, A., 2014. Assessment of Strain Measurement Techniques to Characterise Mechanical Properties of Structural Steel. *Engineering Science and Technology, an International Journal*, 17(4), 260-269.

Palieraki, V., Zeris, C., Vintzileou, E., Adami, C.-E., 2018. In-Plane and out-of Plane Response of Currently Constructed Masonry Infills. *Engineering Structures*, 177, 103-116.

Pan, B., 2018. Digital Image Correlation for Surface Deformation Measurement: Historical Developments, Recent Advances and Future Goals. *Measurement Science and Technology*, 29(8), 082001-082031.

Pan, B., Qian, K., Xie, H., Asundi, A., 2009. Two-Dimensional Digital Image Correlation for in-Plane Displacement and Strain Measurement: A Review. *Measurement Science and Technology*, 20(6), 062001-062017.

Pan, B., Yu, L., Zhang, Q., 2018. Review of Single-Camera Stereo-Digital Image Correlation Techniques for Full-Field 3d Shape and Deformation Measurement. *Science China Technological Sciences*, 61(1), 2-20.

Peters, W.H., Ranson, W.F., 1982. Digital Imaging Techniques in Experimental Stress Analysis. *Optical Engineering*, 21(3), 427-431.

Wu, Z., Guo, W., Pan, B., Kemao, Q., Zhang, Q., 2021. A Dic-Assisted Fringe Projection Profilometry for High-Speed 3d

Shape, Displacement and Deformation Measurement of Textured Surfaces. *Optics and Lasers in Engineering*, 142.

Yamaguchi, I., 1981. Speckle Displacement and Decorrelation in the Diffraction and Image Fields for Small Object Deformation. *Journal of Modern Optics*, 28(10), 1359-1376.

Zhang, Q., Su, X., Xiang, L., Sun, X., 2012. 3-D Shape Measurement Based on Complementary Gray-Code Light. *Optics and Lasers in Engineering*, 50(4), 574-579.

Zhang, S., 2018. High-Speed 3d Shape Measurement with Structured Light Methods: A Review. *Optics and Lasers in Engineering*, 106, 119-131.

Zhang, Z., 1999. Flexible Camera Calibration by Viewing a Plane from Unknown Orientations. *Proceedings of the Seventh IEEE International Conference on Computer Vision*, 1, 666-673.

Zhao, J., Sang, Y., Duan, F., 2019. The State of the Art of Two-Dimensional Digital Image Correlation Computational Method. *Engineering Reports*, 1(2), 12038-12052.